On-surface Double layer polymerization enhancing GNR lengths on an Au(111) surface

Umamahesh Thupakula, We -Hyo Soe, Christian Joachim, Erik Dujardin

On-surface Double layer polymerization enhancing GNR lengths on an Au(111) surface

Umamahesh Thupakula,[a] We-Hyo Soe,[a] Christian Joachim,[a,b] and Erik Dujardin[a,c]

[a]Groupe NanoSciences (GNS), Centre d'Elaboration de Matériaux et d'Études Structurales (CEMES), Centre National de la Recherche Scientifique (CNRS), Université de Toulouse, 29 Rue J. Marvig, BP 94347, 31055 Toulouse Cedex, France.

[b]International Center for Materials Nanoarchitectonics (WPI-MANA), National Institute for Material Sciences (NIMS), 1-1 Namiki, Tsukuba, Ibaraki 305-0044, Japan.

[c]Laboratoire Interdisciplinaire Carnot de Bourgogne, CNRS UMR 6303, Université de Bourgogne Franche-Comté, 9 Av. A. Savary, 21078 Dijon, France.

ABSTRACT

By performing controlled step-by-step annealing experiments of bilayers of GNR monomer reactants with multiple UHV-STM analysis of intermediate stages, we show that the coupling reaction takes place mainly in the uppermost layer of the monomer bilayer despite being separated from the Au(111) surface by the lowermost compact monomer carpet. This demonstrates that the initial monomer bilayer configuration plays acrucial role in lengthening the final GNR length once the intermediate dehalogenated polymer is cyclodehydrogenated. In this respect our experimental results directly provide the counter rationalization to the generalization of the metallic substrate catalytic role in the surface assisted coupling chemical reactions.

INTRODUCTION

On-surface synthesized graphene nanoribbons (GNRs) belong to a recent class of molecular wires anticipated to have tunable electronic structures by varying their length and the chemical structure of their monomer unit precursors.[1-4] First developed by Cai et al., the standard on-surface 7-GNR synthesis protocol is described as a two-step process with initial polyanthryl oligomers formation by an Ullmann coupling reaction followed by a cyclodehydrogenation along the polyanthryl backbone.[5] In solution, the Ullmann-coupling reaction is assisted by metal catalysis.[6-8] On surfaces such as Au(111), Cu(111) or Ag(111), free of solvent and in ultrahigh vacuum (UHV) conditions, the Ullmann coupling reaction also requires the assistance of the metal surface.[9-11] For instance, the dehalogenation process of 10,10'-dibromo 9,9'-bianthracene (DBBA) precursors occurs between 80 °C and 200 °C on Au(111) but is readily observed at room temperature on Cu(111).[12] Likewise, the cyclodehydrogenation step of DBBA takes place at 400 °C on Au(111) but already at 200 °C on Cu(111).[12] The surface mediates the diffusion of the monomers and the chemical intermediates essential to control the kinetics of the on-surface chemical reaction.[13] The surface also plays a central role as a source metallic ad-atoms natively diffusing at room temperature.[14] Finally, the GNR products are maintained in a planar conformation on the surface, thus avoiding any solubility or folding problems.[15]

In this paper, we present a step-by-step study of the on-surface coupling reactions occurring both on the surface and top layer of a 1.5 monolayer (ML) DBBA monomers adsorbed on an Au(111) surface as a function of temperature. Using high resolution LT-UHV STM and STS characterization, we have monitored at every 50 °C, the progress of the on-surface chemical

synthesis of the known 7-aGNR by stopping it at characteristic surface annealing temperatures. This stepwise investigation demonstrates that the Ullmann coupling reaction on a surface not only occurs in the DBBA monomer layer directly in contact with the metal, but also in the upper DBBA layer, electronically decoupled from the surface. The step-by-step interruption of the on-surface reaction enables us to evidence that, prior to the known cyclodehydrogenation step, the polyanthryl oligomers present in the initially self-assembled bilayer nano-islands reorganize into single layer at a very critical temperature. This new intermediate step governs the on-surface synthetic pathway for long GNRs as observed directly from the GNR length distribution and maximum length.

EXPERIMENTAL

Sample Preparation. Au(111) single crystals (*Mateck* GmbH) were used for the on-surface synthesis of GNRs. All samples were prepared in the preparation chamber of our low-temperature ultrahigh vacuum LT-UHV 4-STM instrument (Ref.). The Au(111) surfaces were cleaned under UHV conditions by repeated cycles of Ar^+ ion sputtering at 1.0 keV and ~10^{-6} mbar for about 10 minutes and subsequent annealing at about 740 K for 1 h. The cleanliness, the herringbone reconstruction and the presence of the characteristic surface state of the Au(111) surfaces were checked using one of the STM of our LT-UHV 4-STM operated at the sample temperatures of ~4.5 K. Precursor monomers, '10,10′-dibromo-9,9′-bianthryl (DBBA)' from *Aldrich*, were thermally evaporated from the quartz crucible of a *Kentax* thermal evaporator (*Knudsen*-cell) at 160 °C while the clean Au(111) surface was kept below 40 °C and ca. 50 mm away from the evaporation source. These deposition parameters yielded 0.5 ML, 1.0 ML and 1.5 ML of DBBA in 5, 10 and 30 minutes, respectively (effective coverage measured using large scale STM images). We observe that the effective growth rate deviate from a linear behavior after exceeding 1.0 ML

of DBBA coverage, which might be due to the difference between a monomer/Au(111) (<1.0 ML DBBA) and monomer/monomer/Au(111) (>1.0 ML DBBA) surface adsorption under UHV conditions.

Preparation of the multiple temperature steps on-surface synthesis

Three different DBBA samples coverages (0.5 ML, 1.0 ML and 1.5 ML) on the Au(111) surfaces were first studied before carrying out the step-by-step successive annealing experiments (Figure 1a-c). The surface coverage was derived from the statistical analysis of large scale STM images and not account for the actual monomers evaporation rate from the crucible (see experimental section for more details about sample preparation procedure). After the polymerization (10 minutes, 200 °C) and the cyclodehydrogenation (10 minutes, 400 °C) steps, the monomers were converted in all cases into GNRs as presented in Figure 1d-f. The GNRs appear randomly oriented on the Au(111) surface with a length distribution characterized by the histograms plotted in the insets of Figure 1d-f. For the 1.5 ML case, we observe a fourfold increase in the maximum length of the GNRs on the Au(111) surface compared to 0.5 ML and 1.0 ML as can be clearly observed alongside a broadening of the length distribution. We took benefit of this observation we performed the step-by-step controlled annealing experiments using this 1.5 ML DBBA sample by the steps of 30 minutes at each 50 °C interval between 100 °C and 350 °C until where a well-defined 7-aGNRs were observed on the Au(111) surface. This sequencing of the on-surface chemical reaction requires a back-and-forth travel between the UHV preparation chamber of our LT-UHV 4-STM and the 4-STM stage operating at low temperatures (~4.5 K). For each annealing step this UHV travelling is ~2 m long implying a room temperature thermalization during 10 minutes between the 4-STM LT stage and the sample annealing stage plus another down in

temperature thermalization on its way back to the 4-STM LT stage. In terms of on-surface chemistry, the chemical reaction observation temperature interval was determined by first increasing and then decreasing systematically not to miss an essential on-surface intermediate reaction steps. According to our experimental setup (UHV travelling time, cleanness of the vacuum chamber along the UHV path between the preparation chamber annealing stage and the 4-STM LT stage), a 50 °C step appears an optimum.

STM and STS measurements. All samples were transferred under UHV conditions and characterized *in situ* with the LT-UHV 4-STM instrument (base pressure is $<3\times10^{-11}$ mbar). A lock-in detection technique was implemented to carry out the local density of states (LDOS) measurements by recording both the d*I*/d*V* spectra as well as the d*I*/d*V* maps with open feedback loop conditions (V_{ext} = 16 mV at ~430 Hz). All bias voltages mentioned are with respect to the tip, and with the sample virtually grounded.

For the selected 1.5 ML coverage and before entering in the step-by-step sample annealing at different successive temperatures, large STM images were recorded for reference of the as-deposited 1.5 ML DBBA on the Au(111) surface which clearly show distinct ML and BL monomer regions (Figure 2a). High-resolution STM images reveal a unique interdigitated assembly in ML regions and one-dimensional (1D) linear chain assembly in BL DBBA regions (Figure 2b and 2c). Different samples prepared with this 1.5 ML DBBA coverages exhibit the same distinct self-assembly patterns for ML and BL regions. On the other hand, sub-ML and ML DBBA coverages only showed the same interdigitated assembly patterns on the Au(111) surface as displayed in Figures 1a and 1b. These observations suggest that a specific self-assembly mechanism emerges when the second layer forms on top of the Au(111)-adsorbed lowermost layer. Even though the

DBBA is deposited at Au(111) surface temperatures below 40 °C, annealing at 50 °C has a negligible impact on both ML and BL regions of DBBA (data not shown).

RESULTS

After the initial 1.5 ML deposition and starting by a 100 °C annealing temperature, the DBBA molecules partially desorb from the BL regions creating herringbone-like patterns on the Au(111) surface. The ML regions remain mostly unaffected (Figure 3a). with from place to place point defect like protrusions in the STM corrugation (Figure S1). STS d*I*/d*V* measurements recorded near these protrusions do not reveal any notable tunneling electronic resonances. Therefore, we attribute these protrusions to a surface conformational change of individual DBBA molecules within the self-assembled ML. The remaining BL regions undergo a much more dramatic reorganization, comprising 2D monomer stripe patterns and amorphous aggregates that results from the partial desorption of monomers from the uppermost layer (Figure S1).

At 150°C, the surface monomer desorption proceeds further resulting in a bimodal distribution of smaller BL and larger ML nano-islands (Figure 3b). Additionally, the surface molecular organization is further modified as seen in Figure S2. In ML, the density of protrusions tends to increase while the 1D linear chains of BL regions are fully converted to either 2D periodical stripes or amorphous clumping. These changes reveal a drastic molecular conformational change at the onset of the polyanthryl polymerization.

At ~160-200°C (Figure S3), the knows DBBA molecules Ullmann coupling chemical reaction occurs here with the release of the *Br* and single covalent *C-C* bond formations at each 10 and 10′ sites along the in-formation polyanthryl chains. Figure 3c shows that all the molecular

herringbone-like patterns have vanished thereby exposing a bare Au(111) surface. All molecules chains are now gathered into nano-islands with similar lateral size and uniform apparent STM height (Figure S4). By performing STM molecular manipulations, individual polyanthryl chains can be extracted one by one from those nano-islands demonstrating that the DBBA monomers are now engaged in the progressive formation of the polyanthryl chains. These chains were neither found covalently bonded together by a transverse Ullmann coupling nor by interchain cyclodehydrogenations (Figure S5). Post manipulation STM images are constellated with lone atom-like defects on Au(111) surface that can be easily STM manipulated (Figure S5).

Further information on the oligomer islands molecular structure was gathered using bias-dependent STM imaging. In Figure 4a, an image recorded at +2 V (10 pA) reveals alternate anthracene protrusions on both sides of the oligomer. This specific feature is due to the alternating rotation of adjacent anthracene units around the σ-bonds connecting them owing to their respective steric hindrance. The resulting non-planar conformation displays higher apparent heights at the alternant anthracene sites. When now switching the imaging bias to –2 V (10 pA), a new contrast between adjacent chains appears (Figure 4b). In Figure 4c, the line profile at positive bias presents an ~0.5 nm apparent height with an intrinsic anthracene corrugation. At negative bias, the line scan shows two apparent heights. The higher one at 0.62±0.02 nm is in registry with the anthracene corrugation of the positive bias. The lower one at ~0.48±0.02 nm coincides with the anomalous corrugation at positive bias and reveals the presence of a sub-layer.

May be the following for this temperature in the discussion section?

The origin of this contrast change can be interpreted as a double layer surface molecular structure. Different tunneling mechanisms are involved when tunneling through a polyanthryl

nano-island in the locations where one or two layers are present. Below −1.0 V (Figure S6**)**, the d*I*/d*V* spectra recorded either on top of the 1st layer or on top of the 2nd layer exhibit distinct tunneling electronic resonance patterns. The spectra at the top layer comprise multiple sharp peaks which can be attributed to the inelastic excitation of vibrations in the chains. The spacing between these vibronic replica (labeled V_1,V_2,V_3 and V_4) indicates a dominant vibrational mode with an energy of ~200meV. Such vibronic satellite peaks are absent in the spectrum of the 1st layer with a single broad resonance around ~−1.4 V (Figure S6**)**. Consistently, the d*I*/d*V* map recorded at ~ −1.1 V (i.e. the first resonance V_1) shows an enhanced contrast from the 2nd layer (Figure S6b**)**. The other dI/dV maps recorded at the bias of the satellite peak positions V_2 and V_3 have an identical appearance, thus confirming the vibronic origin of these peaks.

High-resolution STM images at different locations give a ~1.80 ± 0.05 nm inter-chain center distance in the top layer i.e. double the ~0.85 ± 0.05 nm inter-chain distance in the 1st layer (Figures 4d and S7b). A structural model of a polyanthryl nano-island can be proposed where we have identified in red, the molecular chains of the top layer sitting directly on top one out of two chains of the 1st layer (in blue), leaving also a gap between neighboring chains in the uppermost layer (in Figure 4c insert, see also Figure S7a) and Figure 4d).

At ~250 °C, the surface nano-island molecular organization prevails (Figure 3d). Bias polarity dependent Figures 4e and 4f high-resolution STM images characterize the disappearance of the uppermost layer leading to compact side-by-side oligomer chains in a uniform contrast (see also Figure S7c). The line profiles across a nano-island exhibits the same apparent height ~0.51 ± 0.02 nm and ~0.54 ± 0.02 nm at both polarities respectively (Figure 4g**)**. The lateral chain

periodicity is ~0.90 ± 0.05 nm in good agreement with the value measured at the previous annealing step (Figures 4h and S7d**)**.

The d*I*/d*V* spectroscopy (Figure S6c**)** and maps (Figure S6d**)** confirm the absence of the vibronic satellite peaks and of the 2nd layer of the oligomer chains. This indicates that at ~250 °C, the oligomers of the uppermost layer diffuse and sink into the lowermost layer. The resulting structural model of monolayered island is depicted in Figure S7c and inset in Figure 4g.

In Figure 3d, isolated molecular chains can be observed. The high resolution STM images presented in Figure S8 indicate that they are not polyanthryl chains but partially or fully dehydrogenated GNRs with their characteristic planar structure which considerably reduces their STM apparent height. In Figure 4e, a partial GNR is imaged with a ~0.2 nm apparent height (Figure 4g).

Notice that STM measurements reported so far have often showcased isolated GNRs away from the polyanthryl nano-islands and often trapped at the Au(111) herringbone kink sites and oriented along the reconstruction direction. In contrast, Figures 4 and S8 clearly present partially transformed in GNR polyanthryl molecular chains protruding at the periphery of the polyanthryl nano-island. The part of the completed GNR synthesis was extruded out on the free of molecules Au(111) surface locations. We have capture here the cyclodehydrogenation process in progress along the polyanthryl chains located at the periphery of a nano-island rather than for on single polyanthryl chains trapped at Au(111) reactive sites. The completed part of the GNR along a given polyanthryl chain interacts weakly with the polyanthryl nano-islands. Once entirely converted to GNRs, those molecular wires diffuse on the reconstructed Au(111) surface.

Reaching 300°C, all nano-islands are now progressively converted in isolated GNRs as presented in Figure 3e. Stopping the process at 300 °C and using higher resolution STM images

reveals that the cyclodehedrogenation of shorter GNRs (length up to 5-8 nm) is completed whereas longer GNRs retain hydrogenated segments easily identified by their bright spots one side molecular structure. (Figure S9). Here some of the anthracene units along the polyanthryl chains are still hydrogenated (Figure S9b). The GNRs molecular surface coverage is reaching the threshold of its final plateau (see discussion later).

A final annealing at 350 °C complete the cyclodehydrogenationprocess for all the imaged GNRs irrespective of their length (Figures 3f and 5a). Higher resolution STM and d*I*/d*V* spectroscopy (Figure 5b and 5c) and maps (Figure 5d-f) performed on a given isolated GNR of 5 DBBA monomer units in length confirm the presence of the edge states (R0). The first positive (R+1) and negative (R−1) characteristic tunneling resonances (Figure 5c) are indicative of the quantum confinement in a now perfect atomically structured 7-GNR.

DISCUSSION

A detailed assessment of the surface coverage (as presented in the discussion later in Figure 6) showed that the continuous decrease observed at all previous annealing stages is brutally inverted at 250°C. The overall coverage is boosted from 24% to 35% but the nano-island size remains constant while the second layer disappears. These observations concur to a consistent scenario triggered at 250°C: the polyanthryl chains of the uppermost layer migrate into the lowermost layer, the peripheral polymer chains of the lowermost layer are extruded as dehydrogenated GNR leaving the overall lateral size of the islands unchanged but accounting for the disappearance of the second layer and for the appearance of isolated GNRs fully or partially conjugated that contribute to the rebound of the surface coverage.

In order to understand the role of two layered DBBA structure on the GNR lengths, we carried out a twofold analysis of our detailed annealing experiments on 1.5 ML DBBA/Au(111). In the first fold, we calculated and plotted the effective remaining surface coverage of DBBA *vs* annealing temperature (Figure 6**)**. The corresponding plot reveals that the surface coverage decreases drastically until the 200 °C annealing step (dehalogenation and polymerization step) followed by an increase of 10 % each at 250 °C and 300 °C annealing steps. The drastic decrease of surface coverage was, indeed, mainly powered by the monomer desorption from both ML and BL regions of DBBA. However, the STM measurements revealed that, though, monomer desorption is dominated initially from the BL regions (≤100 °C), ML regions disappear completely prior to the polymerization of monomers (between 100°C and 200 °C). Moreover, Ullmann coupling (*via* dehalogenation and polymerization) occurs mainly in the BL patches of DBBA that remained on the Au(111) surface around the polymerization temperatures. As highlighted earlier, second layer of monomers lead the Ullmann type coupling reaction despite the fact that it is separated from the Au(111) surface by the ML carpet of DBBA, creating two layered polymer islands on the Au(111) surface. It is well established that atomically flat metallic surfaces (such as Au(111), Cu(111), and Ag(111), etc.) play a catalytic role in the on-surface synthesis mechanism via assisting the dehalogenation of monomers and stabilizing the intermediate radicals until the polymerization of monomers. However, simultaneous first and second layer polymerization showcase that Ullmann type coupling reaction is still possible in the elevated molecular structures on the metal surfaces. The second layer polymerization of monomers further contribute towards the fractional increment in the surface coverage at 250 °C and 300 °C annealing steps via the reorganization of two-layered to one-layered polymer chain structure. Moreover, two-layered to one-layered reorganization in a

polymer island prior to the transformation into GNRs might indicate that cyclodehydrogenation occurs only in the direct contact configuration between the polymer chains and the metallic Au(111) surface, which is in contrast to indirect coupling chemical reaction occurring in the two layered configuration of monomers. On the other hand, the identical surface coverages at 300 °C and 350 °C annealing steps indicate no major changes occurring at these temperatures except completing the cyclodehydrogenation of polymer chains to produce atomically precise 7-aGNRs (Figure 6**)**.

In the second fold, we analyzed the length distribution of polymer chains and GNRs for 200 °C and 350 °C annealing steps, respectively. Remarkably, the maximum lengths were found to be of the order of ~40-50 nm for both polymers and GNRs (Figure 6**)**.This demonstrates the final GNR lengths are indeed pre-defined at the polymerization step itself and suggests the absence of any further growth phenomenon at the elevated temperatures, such as end-to-end joining of oligomers/GNRs. Moreover, the calculated average size of a polymer island at the 200 °C annealing step is ~50 nm which is also similar to the observed maximum length of oligomers/GNRs. This further point out that the final GNR lengths are defined by their respective double layered island size and shape of DBBA at the polymerization step and which, in turn, is defined by the monomer desorption mechanism prior to the polymerization. This two-fold analysis of controlled annealing experiments highlights that second layer DBBA is assisting the polymerization step by slowing down the monomer desorption mechanism while promoting the maximum possible lengths of polymers/oligomers and GNRs.

Since the presence of second layer DBBA is assisting the polymerization and cyclodehyogenation processes, it is apparent to seek ultra-long GNRs simply by increasing the initial DBBA coverage on the Au(111) surface. For this purpose, we considered higher coverages

of DBBA (>2.0ML) on the Au(111) surface. Surprisingly, the maximum GNR lengths observed for such high coverages of DBBA are still limited to <50 nm. Moreover, the outcome is always a dense packed GNRs (more than a ML) on the Au(111) surface leaving no bare metal surface for GNR manipulation experiments (Figure S10). On the other hand, higher DBBA coverages facilitated the growth of near homogeneous GNRs with a Gaussian distribution pushing to the longer GNR lengths side (Figure S10c). From these observations, we attribute that the initial surface coverage of DBBA beyond 1.5 ML is self-limiting and therefore less significant for the production of ultra-long GNRs.

Our controlled experiments are not just limited to surface coverage parameter, in order to increase further the maximum length of GNRs, we considered and carried out several other controlled experiments, such as, DBBA deposition rate as slow as 0.01 ML/minute (140 °C crucible temperature) and as high as 0.35ML/minute (180 °C crucible temperature) as well as the annealing temperature ramp rate post DBBA deposition as slow as 5 °C/minute and as fast as 25 °C/minute. Additionally, we considered re-deposition of DBBA at the polymerization step on a room temperature deposited sample as well as deposition of DBBA directly at the substrate temperatures of ~200 °C (polymerization step).None of the parameters showed any significant improvement in the observed lengths of oligomer/polymer chains and GNRs. Our wide range of controlled experiments suggested that only surface coverage of monomers between 1.0 ML and 1.5 ML play a key role on the respective GNR lengths and it is less significant for higher coverages of DBBA. Interestingly, thus far, we found only one monomer from the reports, diphenyl-DBBA (DP-DBBA) has shown to produce more than 200 nm long 7-13-aGNRs out of aenormous variety of monomers used for the on-surface synthesis of GNRs till date. It remains to be seen how the

precursor monomer shape and composition impact the long axis only growth kinetics for the production of ultra-long GNRs.

CONCLUSIONS

We have demonstrated the key role played by the monomer BL configuration of DBBA on the GNR length distribution and exremal value, relying on the low-temperature STM and STS measurements. Our deep insights into the on-surface monomer chemical reactions highlight the following conclusions: 1) Only initial surface coverage until the 1.5 ML of DBBA on the Au(111) surface is the crucial parameter that plays the crucial role in enhancing the final length of atomically precise 7-aGNRs. In this process indirect Ulmann type coupling reactions occurring in partially decoupled and elevated 2ndlayer of DBBA, which is separated from the metallic Au(111) surface by the compact monomer 1stlayer, assist the on-surface synthesis kinetics resulting in a fourfold increment in the maximum lengths of GNRs for 1.5 ML coverage compared to the sub-ML initialmonomer coverages. 2) Monomer desorption at the elevated surface temperatures are dominated initially from the BL regions until 100 °C and then from the ML regions between 100° C and 200 °C. The size and shape of monomer BL patches that remained intact on the Au(111) surface just before the Ulmann coupling reaction temperatures define the final GNR length distribution histograms and extremal lengths. 3) In contrast to the indirect Ulmann type coupling reactions favorable in the monomer BL configuration, we observe thatthe single layered polymer chain configuration is favorable for the cyclodehydrogenation process on the Au(111) surface. This phenomenon leads to the reorganization of two-layered polymer islands at ~200 °C into one-layered structure at ~250 °C.4) The cyclodehydrogenation of polyanthryl polymers progresses from the periphery of the one layered polymer island while

pushing the transformed GNR away from the island eventually turning them into well isolated configuration of individual GNRs.

Overall, this work provides the intriguing insights into the well established two-step on-surface synthesis scheme of GNRs on the atomically flat metallic surfaces thus, invoke investigations targeting the role of multilayered on-surface chemical reactions in designing the well controlled 1D, quasi 1D and 2D covalent nanostructures.

ACKNOWLDGEMENTS

U.T. would like to acknowledge Marie Curie Individual Fellowship and funding from H2020 MarieSkłodowska-Curie Actions (GNR CONDUCTANCE project and grantnumber 895239). This work was supported by the European Union Horizon 2020 FET open project "Mechanicswith Molecules" (MEMO, Grant 766864), the University Paul Sabatier (Toulouse, France) andCNRS.

REFERENCES

[1] R. S. K. Houtsma, J. de la Rie, M. Stöhr, *Chem. Soc. Rev.* **2021**, *50*, 6541.

[2] A. Narita, X.-Y. Wang, X. Feng, K.Müllen, *Chem. Soc. Rev.* **2015**, *44*, 6616.

[3] L. Ma, J. Wang, F. Ding, *Chem. Phys. Chem.* **2013**, *14*, 47.

[4] Z. Chen, A. Narita, K.Müllen, *Adv. Mater.* **2020**, *32*, 2001893.

[5] J. Cai, P. Ruffieux, R. Jaafar, M. Bieri, T. Braun, S. Blankenburg, M. Muoth, A. P. Seitsonen, M. Saleh, X. Feng, K. Müllen, R. Fasel, *Nature* **2010**, *466*, 470.

[6] C. Sambiagio, S. P. Marsden, A. J. Blackera, P. C. McGowan, *Chem. Soc. Rev.* **2014**, *43*, 3525-3550.

[7] F. Zhou, J. Guo, J. Liu, K. Ding, S. Yu, Q. Cai, *J. Am. Chem. Soc.* **2012**, *134*, 14326

[8] F. Monnier, M. Taillefer, *Angew. Chem.* **2008**, *47*, 3096.

[9] M. Koch, F. Ample, C. Joachim, L. Grill, *Nat. Nanotechnol.* **2012**, *7*, 713.

[10] K. A. Simonov, A. V. Generalov, A. S. Vinogradov, G. I. Svirskiy, A. A. Cafolla, C. McGuinness, T. Taketsugu, A. Lyalin, N. Mårtensson, A. B. Preobrajenski, *Sci. Rep.* **2018**, *8*, 3506.

[11] C. S. Sánchez, T. Dienel, O. Deniz, P. Ruffieux, R. Berger, X. Feng, K. Müllen, and R. Fasel, *ACS Nano* **2016**, *10*, 8006.

[12] K. A. Simonov, N. A. Vinogradov, A. S. Vinogradov, A. V. Generalov, E. M. Zagrebina, N. Mårtensson, A. A. Cafolla, T. Carpy, J. P. Cunniffe, A. B. Preobrajenski, *J. Phys. Chem. C* **2014**, *118*, 12532.

[13] S. Clair, D. G. de Oteyza, *Chem. Rev.* **2019**, *119*, 7, 4717.

[14] W. Nakanishi, A. Nakata, P. Perez, M. Takeuchi, C. Joachim, K. Sagisaka, *J. Phys. Chem. C* **2021**, *125*, 18, 9937.

[15] V. Georgakilas, J. A. Perman, J. Tucek, R. Zboril, *Chem. Rev.* **2015**, *115*, 4744.

[16] J. Yang, D. Sordes, M. Kolmer, D. Martrou and C. Joachim, *Eur. Phys. J. Appl. Phys.* **2016**, *73*, 10702.

[17] D. G. de Oteyza, A. G.- Lekue, M. V.- Varela, N. M.- Díez, E. C.-Sanroma, M. Corso, G. Vasseur, C. Rogero, E. Guitian, J. I. Pascual, J. E. Ortega, Y. Wakayama, D. Pena, *ACS Nano* **2016**, *10*, 9000.

[18] C. Ma, Z. Xiao, H. Zhang, L. Liang, J. Huang, W. Lu, B. G. Sumpter, K. Hong, J. Bernholc, A.- P. Li, *Nat. Commun.* **2017**, *8*, 14815.

[19] P. Ruffieux, J.Cai, N. C. Plumb, L. Patthey, D. Prezzi, A. Ferretti, E. Molinari, X. Feng, K. Müllen, C. A. Pignedoli, R. Fasel, *ACS Nano* **2012**, *6*, 6930.

[20] X. Su, Z. Xue, G. Li, P. Yu, *Nano Lett.* **2018**, *18*, 5744.

[21] F. Schulz, M. Ijäs, R. Drost, S. K. Hämäläinen, A. Harju, A. P. Seitsonen, P. Liljeroth, *Nat. Phys.* **2015**, *11*, 229.

[22] J. van der Lit, M. P. Boneschanscher, D. Vanmaekelbergh, M. Ijäs, A. Uppstu, M. Ervasti, A. Harju, P. Liljeroth, I. Swart, *Nat. Commun.* **2013**, 4, 2023.

[23] A. Ishii, A. Shiotari, Y. Sugimoto, *Nanoscale* **2020**, *12*, 6651.

[24] C. Moreno, M. V.- Varela, B. Kretz, A. G.- Lekue, M. V. Costache, M. Paradinas, M. Panighel, G. Ceballos, S. O. Valenzuela, D. Peña, A. Mugarza, *Science* **2018**, *360*, 199.

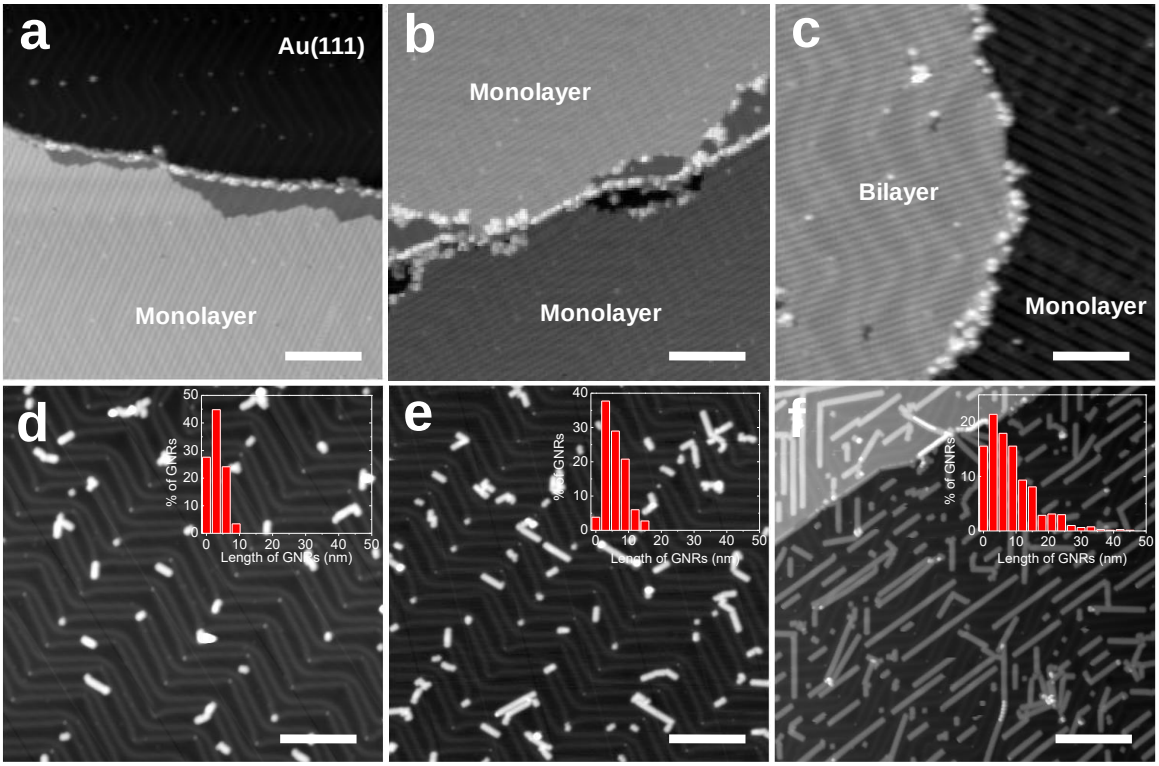

Figure 1: Effect of initial DBBA coverage on the final GNR lengths on the Au(111) surface. **(a-c)** STM topographs showing the self-assembled molecular phase of DBBA at the initial coverages of (a) 0.5 ML, (b) 1.0ML, and (c) 1.5 ML, on the Au(111) surface. (d-f) Corresponding STM topographs after the cyclodehydogenation step revealing the GNRs of the three samples shown in (a-c), respectively. The GNR length histograms are presented in the insets of (d-f). STM set-parameters are +2V/10pA for (a-c) and −2 V/10 pA for (d-f). Scale bars are 20 nm.

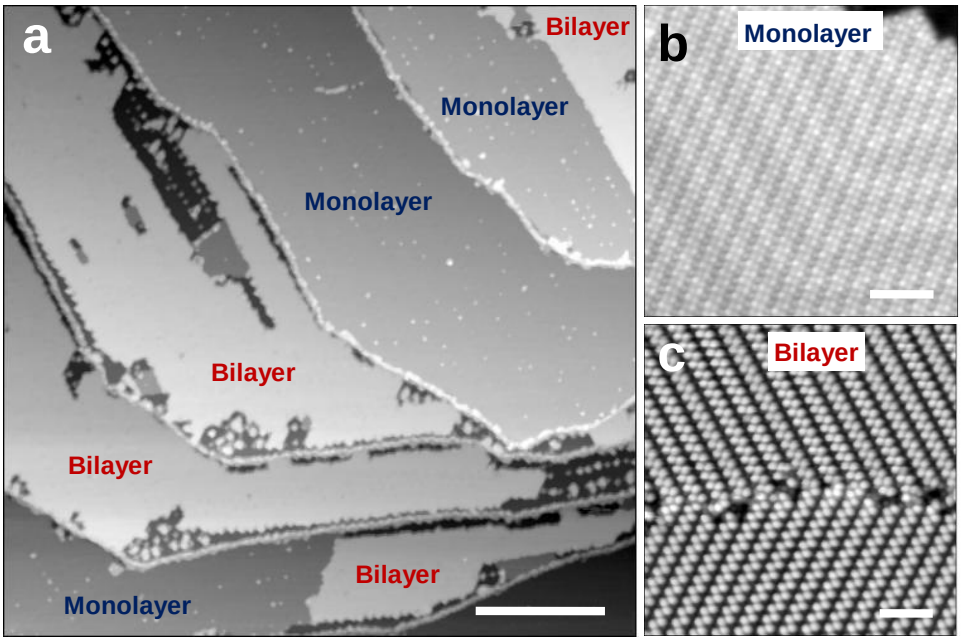

Figure 2: (a) Large-scale STM topograph showing the ML and BL regions of as-deposited 1.5 ML DBBA covered Au(111) surface. The high-resolution STM topographs showcasing the self-assembly patterns of DBBA in the (b) ML and (c) BL regions. STM parameters are +2 V/10 pA. Scale bars are 100 nm for (a) and 5 nm for (b, c).

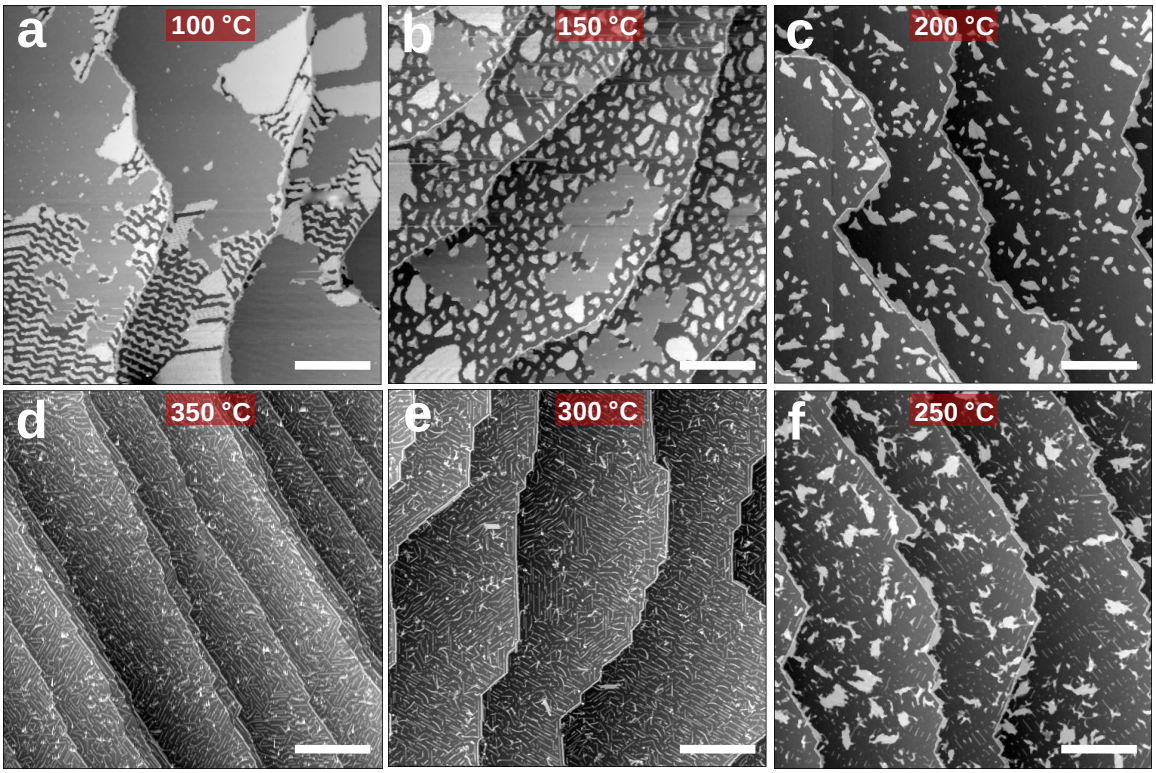

Figure 3: Modification of the sample morphology by stepwise annealing. (a) Large-scale STM topographs revealing the annealing induced surface modifications and structural phase changes in the 1.5 ML DBBA on the Au(111) surface at (a) 100 °C, (b) 150 °C, (c) 200 °C, (d) 250 °C, (e) 300 °C, and (f) 350 °C. STM set-parameters are +2 V/10 pA (a-c) and −2 V/10 pA (d-f). Scale bars are 100 nm.

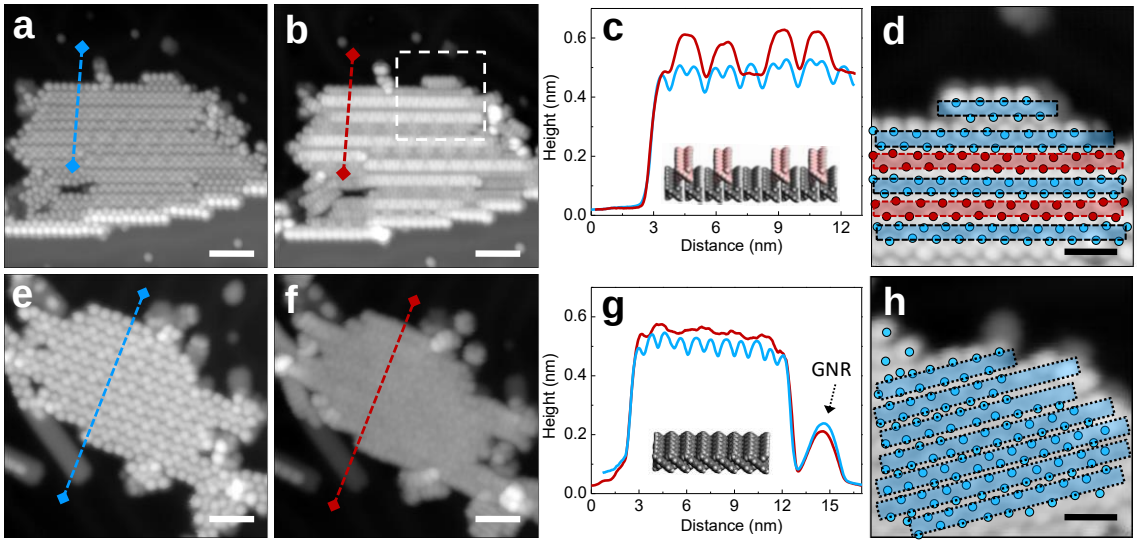

Figure 4: Bias polarity dependent apparent appearance of polyanthryl polymer island on the Au(111) surface. High-resolution STM topographs recorded after the 200 °C annealing step showing the distinct morphology of a polymer island at the positive bias of (a) +2.0 V/10 pA and at the negative bias of (b) −2.0 V/10 pA. Corresponding line profiles drawn across the polymer island in (a) and (b) are presented with a blue and a red curve in (c), respectively. A reconstructed ball model of two layered polymer structure is given in the inset of (c). (d) An overlaid schematic on the high-resolution STM image showing the 1st layer and 2nd layer polymer chains in blue and red colored frames, respectively. Each isolated frame corresponds to a polymer chain in (d). Bias polarity dependent high-resolution STM topograph analysis carried out at the 250 °C annealing step presented in (e-h) resemble the 200 °C annealing step presented in (a-d), respectively. Scale bars are 5 nm.

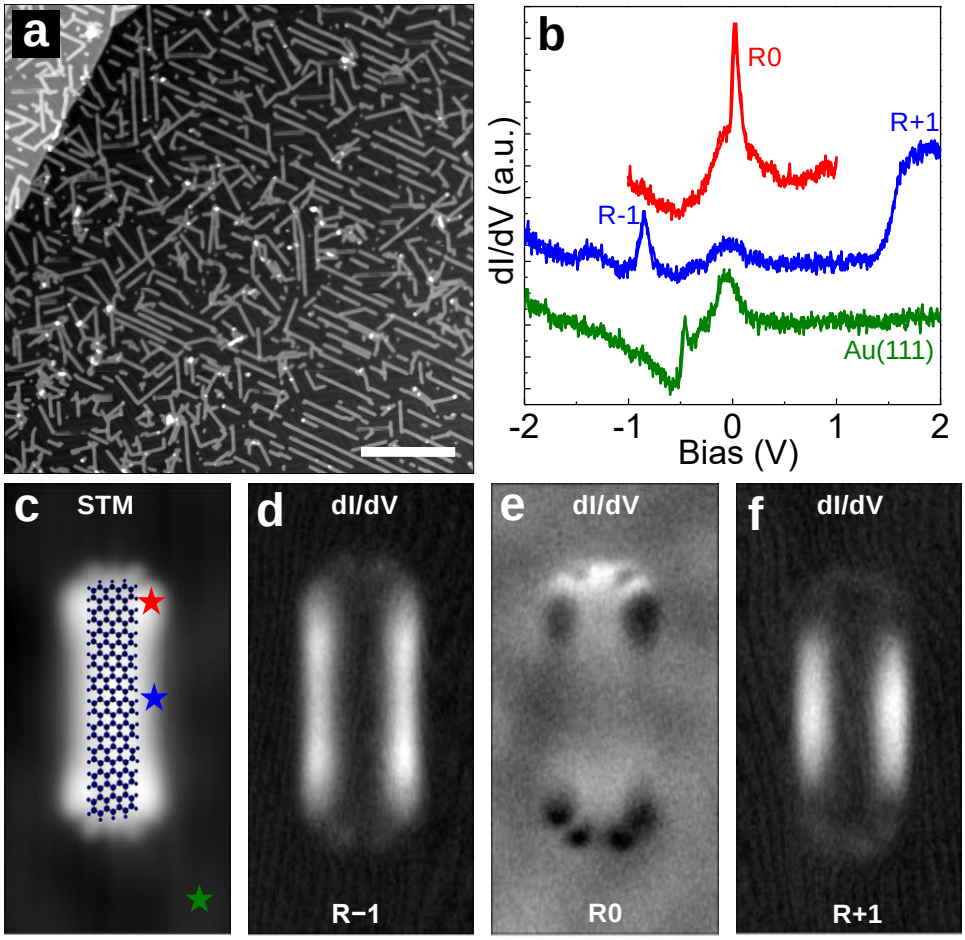

Figure 5: LDOS characteristics of individual GNR and surface coverage plot. (a) Large-scale STM image after the 350 °C annealing step showing completely transformed GNRs on the Au(111) surface. STM set-parameters are −2.0 V/10 pA. (c) The d*I*/d*V* tunneling spectra of an example GNR derived from (c) 5 DBBA monomer units and (d-f) corresponding d*I*/d*V* maps (LDOS) revealing the edge state resonance (R0) and characteristic first resonances at the negative (R−1) and the positive (R+1) bias voltages. A characteristic Au(111) reference spectrum (green) was also included in (b). Corresponding spectroscopic positions are marked with colored stars in the STM image (c). A ball model schematic of 5-aGNR was overlaid in the STM image in (c).

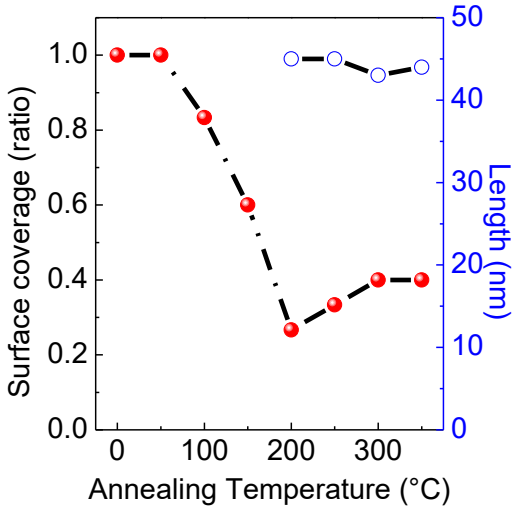

Figure 6: (a) The plot showing the respective surface coverage remained after each annealing step (red dot and black line) of 1.5 ML DBBA on the Au(111) surface. Corresponding maximum polymer/GNR length observed at their respective annealing temperatures is indicated with open blue circle and black line.